Journal of Metals, Materials and Minerals, 37(1), e2496, 2027

A Bi-Mn based ceramic with tunable electrical properties for high temperature NTC-thermistor application

Nusrat ZAHAN[1], Praveen Priyaranjan NAYAK[1,*], Rashmi Rani PATRO[2], Siddharth SAHANY[1], Debasish PANDA[3], Om Prakash DAS[1], and Sushansu Sekhar HOTA[3]

[1] *Faculty of Engineering and Technology, SOA University, BBSR, India*
[2] *Department of Computer Science & Information Technology (CSIT), GITA Autonomous College, BBSR, India*
[3] *Department of Physics, SOA University, BBSR, India*

***Corresponding author e-mail**: praveennayak@soa.ac.in

Received date:
29 August 2025
Revised date:
18 March 2026
Accepted date:
22 May 2026

Keywords:
$BiMn_2O_5$-Sillenite;
Dielectric;
High-T thermistor;
Impedance

Abstract

This article presents detailed structural and electrical properties of $BiMn_2O_5$-Sillenite biphasic ceramic synthesized via solid state reaction technique. The weight percentage of $BiMn_2O_5$ and $Bi_{25}Mn_2O_{40}$ are found to be 90.121 ± 1.900 and 9.878 ± 0.022, respectively. The scanning electron microscope image of the composite material that reflects the presence of polycrystalline nature having the average grain size (G_{avg}) 1.22 µm. The topographic grain behaviour shows the presence of high intense grains nature of the material surface. We investigated relaxation processes, ionic hopping, transport mechanisms, and semiconducting properties by studying the dielectric, conductivity, modulus, and impedance spectra over a broad frequency range (1 kHz to 1 MHz) and temperatures from 25°C to 500°C. The thermistor constant (β) is 2053.8, and the temperature coefficient of resistance (TCR) is found to be –0.00253 which confirms the suitable NTC properties. The NTC behaviour confirms the material is very good candidate for high-T thermistor component.

1. Introduction

A high dielectric constant and stable performance across temperatures are crucial for the ceramic capacitor industry. As advanced electronic materials are developed, electronic devices are expected to function reliably over broader temperature ranges. To meet the demands of increasingly compact electronics, capacitors must maintain both a high dielectric constant and strong thermal stability. Numerous strategies, particularly dopant engineering, have been employed to enhance both the dielectric constant and the temperature resilience of capacitor materials [1]. Compounds possessing high as well as low dielectric constant are generally preferred due to their active and passive applications in thermistors, transducers, capacitors, microelectronics, etc [2]. For decades, materials in the RMn_2O_5 family (where R represents rare earth elements, yttrium, or bismuth) have drawn considerable scientific interest owing to their unique multiferroic behavior, including magneto-electric and magneto-dielectric effects [3], The magnetic oxide $BiMn_2O_5$ is a member of the RMn_2O_5 family, and it crystallizes in the orthorhombic structure (space group Pbam).

Earlier studies revealed that $BiMn_2O_5$ (BMO) displays distinct magnetic behavior compared to other RMn_2O_5 compounds, prompting detailed research into its structure and magnetism, especially at low temperatures [4,5]. In BMO, Mn^{4+} and Mn^{3+} ions exhibit short-range magnetic order below the phase transition, with specific Mn–O–Mn couplings resulting in a commensurate magnetic structure [6]. Additionally, BMO shows dielectric, pyroelectric, and ferroelectric properties below 290 K due to highly polarizable Bi^{3+} ions [7]. To improve its multiferroic and multifunctional characteristics, Bi^{3+} has been partially replaced with rare earth ions like Ce^{3+} [8] and Eu^{3+} [9]. Notably, Ce-doped BMO becomes ferromagnetic at low temperatures, unlike the antiferromagnetic parent compound. Ti-doped BMO has also been studied for its enhanced magnetic, dielectric, and electronic properties [10].

The presence of Bi contents develops cubic sillenite phase ($Bi_{24}Mn_2O_{40}$) in the material BMO [11]. The cubic sillenite phase has also influenced other physical and electrical properties.

The sillenite phase $Bi_{24}Mn_2O_{40}$ is a cubic-structured bismuth manganate compound synthesized hydrothermally, featuring Mn^{4+} (possibly Mn^{5+}) in tetrahedral sites [12]. Sillenite phases like $Bi_{24}Mn_2O_{40}$ exhibit intriguing electrical properties due to their noncentrosymmetric structure, including photoconductivity and potential high-temperature piezoelectricity, akin to related $Bi_{25}FeO_{40}$ analogs with photocurrent densities around 0.37 µA·cm^{-2} [13,14]. Dielectric characteristics show thermally activated relaxation, with anomalies observed near 671 K in similar iron-sillenites; $Bi_{24}Mn_2O_{40}$ likely displays frequency-dependent permittivity and low conductivity influenced by Mn-Bi-O bonding [15].

The motivation of the work is to investigate structural, topographical, dielectric and electrical properties of the biphasic ceramic (Sillenite phase influenced with BMO) for used in NTC application.

2. Synthesis and characterization

The $BiMn_2O_5$-Sillenite compound was prepared via the conventional solid-state reaction technique. High-purity bismuth oxide (Bi_2O_3,

99%, LOBA CHEMIE) and manganese oxide (Mn_2O_3, 99%) were thoroughly blended for 5 h using an agate mortar and pestle to ensure homogeneity. The resulting mixture was subjected to calcination at 850°C for 5 h in a high-purity alumina crucible. Phase identification was carried out using an X-ray diffractometer (Rigaku Ultima IV) equipped with a CuKα radiation source.

Following the phase analysis, the powder was compressed into disc-shaped pellets (12 mm diameter, 1 mm to 2 mm thick) using a KBr hydraulic press for subsequent electrical testing. These pellets underwent sintering at 900°C for 4 h in a muffle furnace to enhance densification. Silver paste of high purity was applied to both faces of the sintered samples to serve as electrodes before connecting them to the impedance analyzer.

Electrical and dielectric properties were assessed over a wide frequency range (1 kHz to 1 MHz) and temperature span (25°C to 500°C) using a computerized LCR meter setup. The surface microstructure of the sintered specimen was examined through scanning electron microscopy (SEM, M/s ZEISS), and elemental composition was investigated using energy-dispersive X-ray spectroscopy (EDX).

3. Results and discussion

3.1 Structural and topographical analysis

Figure 1(a) presents the X-ray diffraction pattern at room temperature for the calcined BMO-Sillenite powder. The reliable parameters are found to be R_b (%) = 10.28, R_e (%) = 8.766 and the sig. value is 1.463. The weight percentage of $BiMn_2O_5$ and $Bi_{25}Mn_2O_{40}$ are found to be 90.121 ± 1.900 and 9.878 ± 0.022, respectively. Figure 1(b) shows the scanning electron microscope image of the composite material that reflects the presence of polycrystalline nature having the average grain size (G_{avg}) 1.22 µm. The topographic surface of the BMO-Sillenite material is shown in Figure 1(c). That shows the occurrence of high intense grains nature of the material surface. The surface-roughness parameters are calculated through *Mountains software* [16] shown in Figure 1(d).

Here, Sq represents the root mean square (RMS) surface height, Ssk indicates the skewness of the height distribution, and Sku describes its kurtosis. Sp corresponds to the maximum peak height, while Sv, Sz, and Sa denote the maximum valley depth, total height, and average surface roughness, respectively [17].

3.2 Dielectric and conductivity study

Dielectrics function as electrical insulators that undergo polarization when exposed to an external electric field. Unlike conductive materials, dielectrics do not allow free electron flow; instead, their internal charges undergo microscopic displacements to form electric dipoles. This internal polarization partially counteracts the applied field, which effectively boosts the ability of the material to store charges, or its capacitance. The process is driven by three primary mechanisms: electronic, atomic, and orientational polarization, each dictated by the specific molecular arrangement of the substance. A performance of the material in these applications is quantified by its dielectric constant (relative permittivity). In modern electronics, high-permittivity dielectrics are vital for optimizing semiconductor devices and integrated circuits, as they help maintain high performance while significantly reducing energy loss through leakage currents.

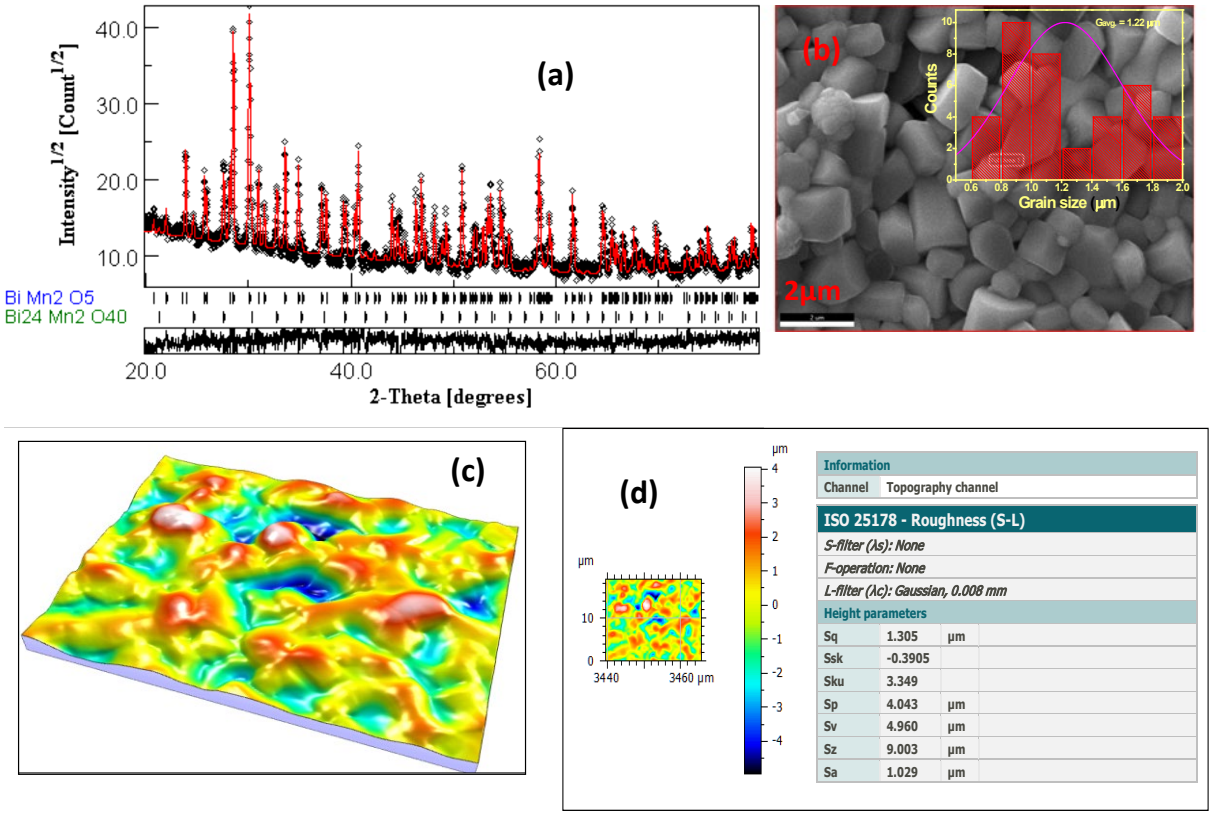


Figure 1. (a) Reitveld analysis, (b) SEM analysis, (c) topographic image, and (d) surface-roughness parameter of BMO-Sillenite material.

As depicted in Figure 2(a), the value is elevated at low frequencies and levels off as frequency increases. At higher frequencies, the observed decrease in dielectric constant is attributed to electronic polarization effects. Figure 2(b) shows the loss tangent (tanδ) changes with temperature from 25°C to 500°C. In this figure, at low frequency (1 kHz) shows the highest loss values. This is because at lower frequencies, dipoles and even slower-moving ions/vacancies have more time to align with the field, leading to more significant energy dissipation whereas, at high frequency (1 MHz) shows the lowest loss values. At high speeds, only the lightest/fastest dipoles can react, and the slower mechanisms (like space charges) cannot keep up, resulting in lower measured loss.

If we look closely at the first major peak (around 180°C to 220°C), we noticed that as the frequency increases, the peak shifts toward higher temperatures. This is a classic sign of thermally activated relaxation [18]. To keep up with a faster-alternating field (higher frequency), the material requires more thermal energy (higher temperature) to speed up the dipole rotation. After 300°C, all curves begin to trend upward significantly. This suggests that the material becomes more conductive at high temperatures. Figure 2(c) displays the variation of ac conductance with frequency at different temperatures. The ac conductance (σ_{ac}) is calculated using the formula: $\sigma_{ac} = 2\pi f\varepsilon_r\varepsilon_0\tan\delta$. At lower frequencies, σ_{ac} stays relatively constant, but it rises as the frequency increases. The increase in conductivity with temperature is likely due to the movement of free charges across grain boundaries, which are evenly distributed throughout the ceramic material [19].

3.3 Complex Impedance and modulus study

Impedance spectroscopy is used to explore the impact of micro-structural characteristics on the material's electronic properties over a wide range of frequencies and temperatures. In this analysis, the complex components of impedance are examined.

$$Z^* = |Z| \times \cos\theta - j \times |Z| \times \sin\theta = Z' + j\,Z'' = \left[\frac{R}{1+(\omega\tau)}\right] + j \times \left[\frac{-\omega R^2 C}{1+(\omega\tau)^2}\right] \quad (1)$$

Here, In the given expression, (Z^*) represents the complex impedance, while (|Z|) denotes the magnitude of impedance and (θ) is the phase angle. The terms (Z′) and (Z″) correspond to the real (resistive) and imaginary (reactive) components of impedance, respectively. Here, (R) stands for resistance, (ω) is the angular frequency (ω = 2πf), (τ) is the time constant (τ = RC), and (C) represents capacitance of the material, respectively.

Figure 3(a) shows the Nyquist plot (Z′ vs Z″), highlighting the contributions from grains, grain boundaries, and electrode effects within the material. The experimental data were compared with theoretical values using ZSIMPWIN (2.0) software. As temperature increases, a semicircular arc appears in the plot. Various RC circuit models were applied to fit the Nyquist data, and the resulting fit (CQR) closely matches the experimental results. Here Q represents the constant phase element of the circuit. The presence of a single arc in the impedance spectra indicates the material exhibits grain dominating characteristics.

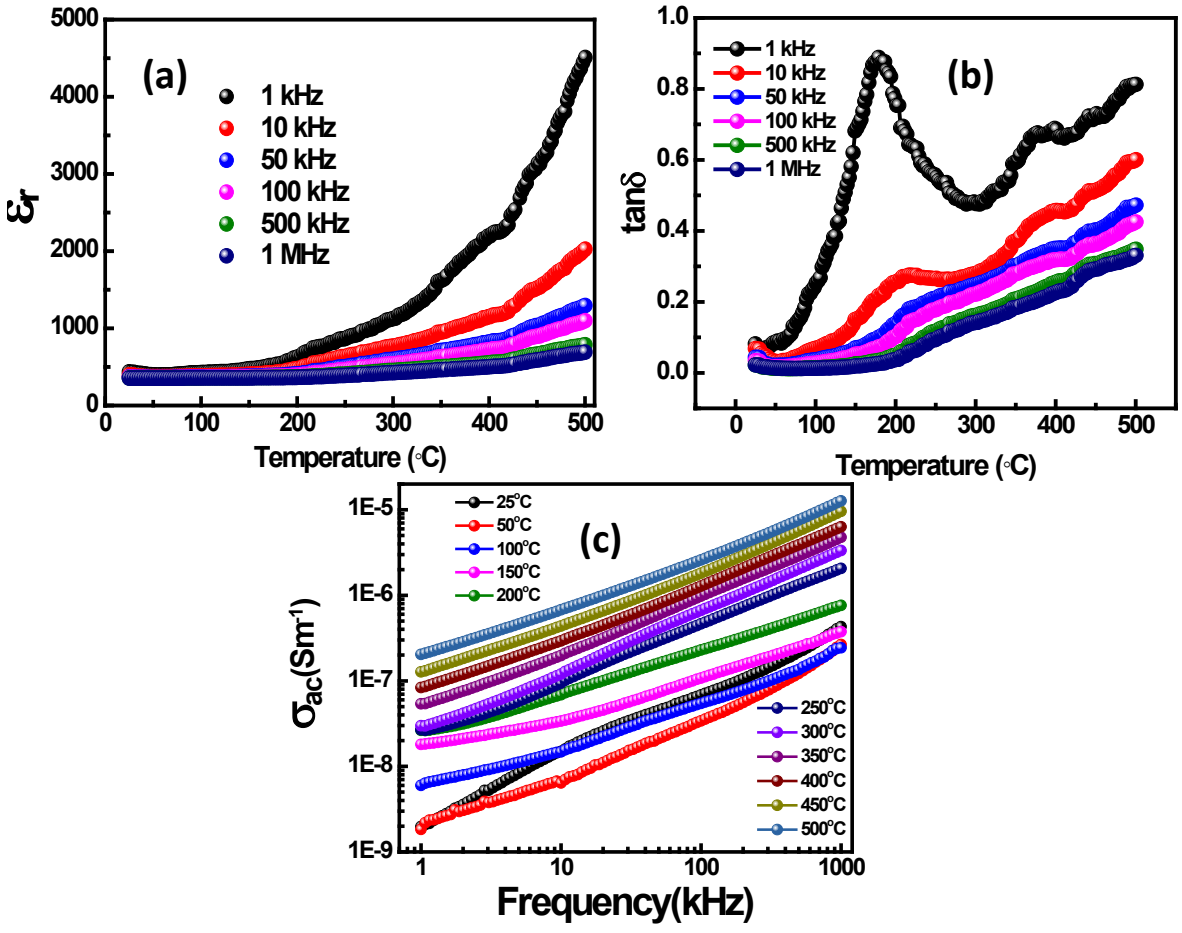


Figure 2. (a) Temperature dependence of ε_r, (b) tanδ, and (c) frequency dependence of σ_{ac} of BMO-Sillenite material.

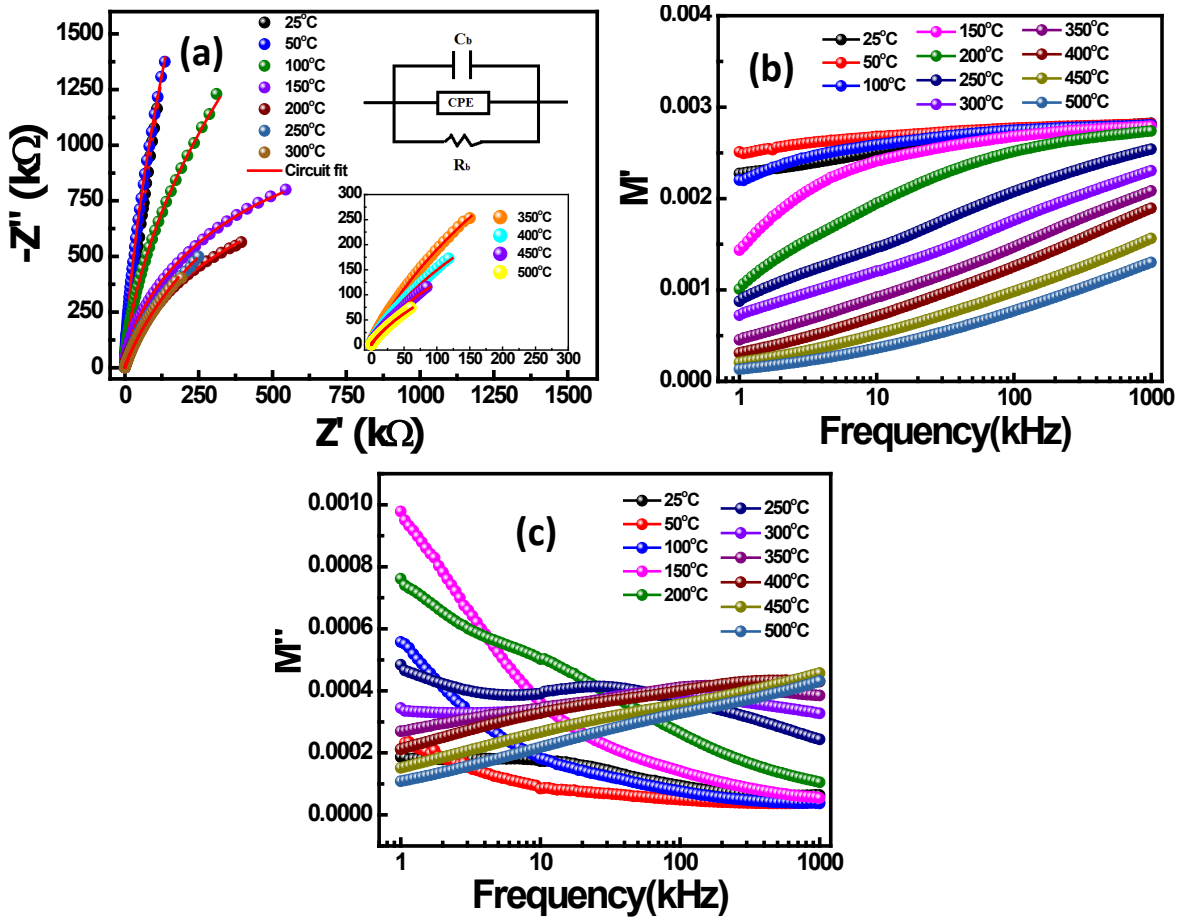


Figure 3. (a) Nyquist plot, (b) frequency dependence of M' , and (c) M″ of BMO-Sillenite material.

The complex modulus spectra are obtained through mathematical analysis of the impedance measurements, and can be represented by the following equation:

$$M^{*} = \omega C_0 \left[\omega R^2 C/\left(1 + (\omega\tau)^2\right)\right] + \omega C_0 \left[R/(1 + (\omega\tau)^2\right] \qquad (2)$$

Where C0 = ε0A/d, ε0, d, and A are the permittivity, thickness, and area of the material.

At lower frequency ranges in Figure 3(b), every temperature shows real modulus (M′) values nearing null, which results from the negligible influence of electrode polarization. The conduction process is governed by the movement of localized charge carriers that are not subject to a restoring force. By analyzing the frequency-dependent imaginary part of the modulus (M″), as shown in Figure 3(c), insights into both conduction and relaxation behaviors can be gained. The shift in M″ peak positions with temperature demonstrates the presence of thermally activated relaxation. Furthermore, the shape of these spectra suggests that the relaxation does not follow the typical Debye model [20].

3.4 NTC thermistor analysis

A thermistor sensor functions by exhibiting resistance that varies with temperature. NTC (negative temperature coefficient) thermistors are temperature-sensitive resistors whose resistance decreases with rising temperature [21-23]. Known for high sensitivity, accuracy, nd quick response, they are ideal for precise temperature control. They are widely used in thermometers, battery systems, HVAC units, and electronics, while also protecting circuits by limiting inrush current and enhancing overall device reliability. This section examines the relationship between resistance and temperature. Figure 4(a) illustrates how resistance changes across the 150°C to 500°C (423 K to 773 K) range. The observed decrease in resistance with rising temperature is characteristic of materials with a negative temperature coefficient of resistance (NTCR).

To grasp how thermistors function, it is essential to evaluate specific material characteristics, including the thermal sensitivity of resistance (TCR) and the β parameter. The β and TCR value are calculated through the equation given below.

$$\beta_{(423/733\ \mathrm{K})} = \frac{In\frac{R_{423\ \mathrm{K}}}{R_{773\ \mathrm{K}}}}{\frac{1}{T_{423\ \mathrm{K}}} - \frac{1}{T_{773\ \mathrm{K}}}} \quad \text{and}$$

$$\mathrm{TCR}_{(423/733\ \mathrm{K})} = \frac{1}{T_{773\ \mathrm{K}} - T_{423\ \mathrm{K}}}\left[\frac{R_{773\ \mathrm{K}} - R_{423\ \mathrm{K}}}{R_{423\ \mathrm{K}}}\right]$$

R_{423K} and R_{773K} correspond to the resistance values at 423 K and 773 K, while T_{423K} and T_{773K} indicate the respective temperatures. The calculated thermistor constant (β) is 2053.8, and the temperature coefficient of resistance (TCR) is –0.00253. Figure 4(b) explores how the logarithm of resistance varies with temperature, revealing a straight-line trend. This linear decrease in ln (R) with rising temperature confirms the material's strong potential as an NTC thermistor, making it highly suitable for use in high-temperature sensor applications [24-27].

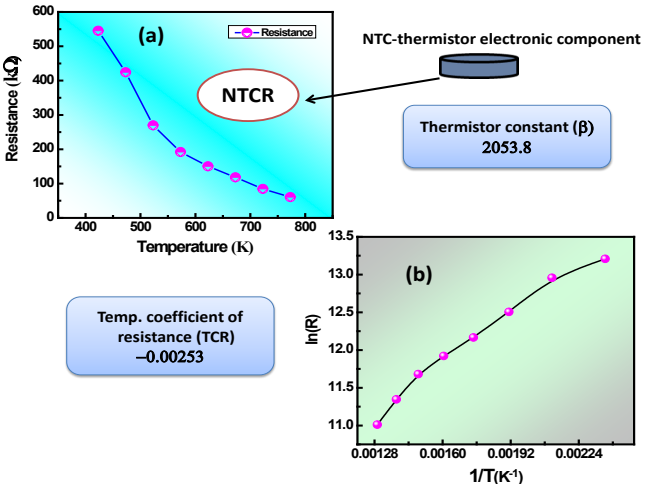


Figure 4. (a) Resistance behaviour with temperature, and (b) Ln(R) vs. Inverse temperature of BMO-Sillenite.

4. Conclusion

A biphasic $BiMn_2O_5$-Sillenite material is synthesized via solid-state route. The Reitveld analysis confirms the presence of $BiMn_2O_5$ (90.121 ± 1.900 wt%) and $Bi_{25}Mn_2O_{40}$ (9.878 ± 0.022 wt%). The microstructural study confirms the presence of polycrystalline nature having the average grain size (G_{avg}) 1.22 µm. The comparative high dielectric constant and low loss (<1) shows a promising tuning electrical properties of $BiMn_2O_5$-Sillenite. The presence of a single arc in the impedance spectra indicates the material exhibits grain dominating characteristics. The temperature-dependent resistance analysis divulges the material is superior candidate for high-temperature NTC thermistor and other temperature-dependent electronic device applications.

Data accessibility

The author will provide the study data upon a valid request.

Declaration of Competing Interest

No any competing personal and financial Interest.

Acknowledgment

The authors are thankful to SOA (DU), Odisha, India for all experimental facilities

References

[1] D. Maurya, F. C. Sun, S. P. Alpay, and S. Priya, "A new method for achieving enhanced dielectric response over a wide temperature range," *Scientific reports*, vol. 5, no. 1, p. 15144, 2015.

[2] C. Sun, J. A. Alonso, and J. Bian, "Recent advances in perovskite-type oxides for energy conversion and storage applications," *Advanced Energy Materials*, vol. 11, no. 2, p. 2000459, 2021.

[3] N. Hur, S. Park, P. A. Sharma, S. Guha, and S. W. Cheong, "Colossal magnetodielectric effects in $DyMn_2O_5$," *Physical review letters*, vol. 93, no. 10, p. 107207, 2004.

[4] N. E. Massa, A. F. García-Flores, D. D. S. Meneses, L. Del Campo, P. Echegut, G. F. Fabbris, M. J. Martinez-Lope, and J. A. Alonso, "Collective phase-like mode and the role of lattice distortions at TN ~ TC in RMn_2O_5 (R= Pr, Sm, Gd, Tb, Bi)," *Journal of Physics: Condensed Matter*, vol. 24, no. 19, p. 195901, 2012.

[5] A. F. García-Flores, E. Granado, H. Martinho, R. R. Urbano, C. Rettori, E. I. Golovenchits, V. A. Sanina, S. B. Oseroff, and S. W. Cheong, "Anomalous phonon shifts in the paramagnetic phase of multiferroic RMn_2O_5 (R=Bi, Eu, Dy): Possible manifestations of unconventional magnetic correlations," *Physical Review B*, vol. 73, no. 10, p. 104411, 2006.

[6] K. S. Kumar, and C. Venkateswaran, "Effect of Fe substitution on the magnetic properties of $BiMn_2O_5$," *Journal of Physics D: Applied Physics*, vol. 44, no. 32, p. 325001, 2011.

[7] I. D. Zhitomirskii, N. E. Skorokhodov, A. A. Bush, O. I. Chechernikova, V. F. Chuprakov, and Y. N. Venevtsev, "Dielectric, pyroelectric and magnetic properties of $BiMn_2O_5$ crystals," *Fizika Tverdogo Tela*, vol. 25, no. 3, pp. 953–955, 1983.

[8] Z. H. Sun, B. L. Cheng, S. Dai, K. J. Jin, Y. L. Zhou, H. B. Lu, Z. H. Chen, and G. Z. Yang, "Effect of Ce substitution on magnetic and dielectric properties of $BiMn_2O_5$," *Journal of applied physics*, vol. 99, no. 8, p. 084105, 2006.

[9] R. A. Ferreira, M. E. Dos Santos, C. Morilla-Santos, R. Lebullenger, O. Peña, and P. N. Lisboa-Filho, "Effect of Eu substitution on the crystallographic and magnetic properties of the $BiMn_2O_5$ oxide obtained by urea combustion," *Ceramics International*, vol. 40, no. 8, pp. 13643–13648, 2014.

[10] D. K. Shukla, S. Mollah, R. Kumar, P. Thakur, K. H. Chae, W. K. Choi, and A. Banerjee, "Effect of Ti substitution on multi-ferroic properties of $BiMn_2O_5$," *Journal of Applied Physics*, vol. 104, no. 3, p. 033707, 2008.

[11] K. Annamalai, R. Radha, S. E. Kichanov, M. Navaneethan, and S. Balakumar, "Ice bath assisted $BiMn_2O_5$(Mullite) Phase synthesis, structural and compositional analysis under different Bi concentration," *ECS Journal of Solid State Science and Technology*, vol. 10, no. 6, p. 061001, 2021.

[12] T. I. Mel'nikova, G. M. Kuz'micheva, V. B. Rybakov, N. B. Bolotina, and A. B. Dubovsky, "Synthesis, composition, and structure of sillenite-type solid solutions in the Bi_2O_3– SiO_2–MnO_2 system," *Inorganic Chemistry*, vol. 50, no. 5, pp. 2002–2009, 2011.

[13] R. Shukla, P. Saha, A. B. Shinde, P. S. R. Krishna, P. D. Babu, A. K. Tyagi, S. N. Achary, D. Santamaria-Perez, T. Marqueno, J. Ruiz-Fuertes, C. Popescu, and D. Errandonea, "On formation and evolution of structure of sillenite type $Bi_{25}FeO_{40}$ phase with temperature and pressure," *Journal of Alloys and Compounds*, vol. 1020, p. 179528, 2025.

[14] J. Xue, H. Zhang, J. Han, and Y. Ling, "Thermal, magnetic and photoelectrical behaviors of sillenite $Bi_{25}FeO_{39}$ microcrystals," *Ceramics International*, vol. 47, no. 7, pp. 9941–9947, 2021.

[15] J. S. Cha, and K. Park, "Sol-gel synthesis, microstructure, and thermoelectric properties of $Ca_{2.8-x}Bi_xDy_{0.2}Co_4O_{9+\delta}$," *Ceramics International*, vol. 43, no. 18, pp. 16159–16166, 2017.

[16] J. Hansen, "Assessing the tribological interface of mechanical parts," *Surface Newsletter (Digital Surf)*, pp. 6–7, 2020.

[17] D. Panda, S. S. Hota, and R. N. P. Choudhary, "Investigation of structural, topological, and electrical properties of scheelite strontium molybdate for electronic devices," *Inorganic Chemistry Communications*, vol. 158, p. 111501, 2023.

[18] D. Panda, S. S. Hota, and R. N. P. Choudhary, "Investigation of the structural, surface topographical, fractal, capacitive, and electrical properties of a defect brownmillerite perovskite material $KBiFeMnO_5$ for electronic devices," *RSC advances*, vol. 14, no. 5, pp. 3400–3412, 2024.

[19] C. R. Mariappan, "AC conductivity scaling behavior in grain and grain boundary response regime of fast lithium ionic conductors," *Applied Physics A*, vol. 117, pp. 847–852, 2014.

[20] M. B. Bechir, M. Akermi, and H. J. Alathlawi," Understanding charge transport and dielectric relaxation properties in lead-free Cs_2ZrCl_6 nanoparticles," *RSC advances*, vol. 14, no. 20, pp. 14221–14232, 2024.

[21] S. S. Hota, D. Panda, L. Biswal, S. Joshi, A. Shukla, and R. N. P. Choudhary, "Effect of milling time on structural and electrical properties of thermomechanically synthesized of $Ba_{0.1}(Bi_{0.45}Na_{0.45})TiO_3$ nanoceramics for ferroelectric random-access memory device," *Journal of Alloys and Compounds*, vol. 1010, p. 177041, 2025.

[22] S. S. Hota, D. Panda, and R. N. P. Choudhary, "Structural, dielectric, electrical, and leakage current properties of $SrWO_4$ for electronic devices," *Journal of the Korean Ceramic Society*, vol. 61, no. 6, pp. 1207–1221, 2024.

[23] D. Panda, S. S. Hota, and R. N. P. Choudhary, "Development of lead-free defect brownmillerite perovskite ceramic $LiBiFeMnO_5$ solid solution for electronic devices," *Advanced Engineering Materials*, vol. 26, no. 20, p. 2400010, 2024.

[24] R. Wu, Z. Fu, Y. Liu, Y. Wei, H. Sun, A. Chang, and B. Zhang, "Widening the temperature range and improving the linearity of $CaCu_3Ti_4O_{12}$ ceramics for high-temperature NTC thermistor application through entropy engineering strategy," *Journal of Alloys and Compounds*, vol. 973, p. 172908, 2024.

[25] P. Agnihotri, R. Rai, S. Kumari, and R. Goel, "Exploring NTC thermistor properties of $La_{0.665}Bi_{0.33}Ba_{0.005}Gd_{1-x}Mn_xO_3$," *Transactions on Electrical and Electronic Materials*, vol. 26, pp. 573–589, 2025.

[26] H. Xiao, C. Liu, T. Zheng, Y. Liu, and Y. Lyu, "$(1-x)Ni_{0.9}Mn_{2.1}O_{4-x}LaCr_{0.6}Mn_{0.4}O_3$ composite ceramic with controllable electrical properties for low resistance NTC thermistors," *Journal of Alloys and Compounds*, vol. 1000, p. 175085, 2024.

[27] L. Wu, J. Wang, G. Lan, W. Li, P. Meng, and S. Jia, "$BaTiO_3$-$BiMnO_3$ perovskite NTC thermistors for high-temperature batteries," *Journal of Alloys and Compounds*, vol. 1011, p. 178396, 2025.